Crystallization of the One-Component Plasma at Finite Temperature

M. D. Jones and D. M. Ceperley

Department of Physics, National Center for Supercomputing Applications, University of Illinois at Urbana-Champaign, Urbana, Illinois 61801

(Received 16 January 1996)

We have determined the coexistence at positive temperature between a Wigner crystal and a fluid plasma using path integral Monte Carlo. The total energies are significantly different from classical and semiclassical predictions. The location of the phase transition between liquid and solid is higher in temperature than predicted by a generalized Lindemann criterion. Some features of the phase diagram can be understood using a novel application of the Clausius-Clapeyron equation. We find a maximum melting temperature of $6.0(5) \times 10^{-5}$ Ry at $r_s \simeq 180(20)$. [S0031-9007(96)00437-1]

PACS numbers: 71.10.Ca, 68.35.Rh, 64.70.Dv, 67.90.+z

An important model in the study of many body systems is the one-component plasma (OCP), which consists of some type of charged particle (an atomic nucleus, for example), and a rigid neutralizing background. When the particles are fully ionized atoms, the OCP is thought to be a good approximation to the interiors of compact stellar remnants such as white dwarfs. Crystallization plays an important role in the evolution of such objects [1] since the cooling rate for white dwarfs strongly depends on the phase of the matter in the star—whether free thermal motion or lattice vibrations are the central cooling mechanism. Equivalently, if the particles are electrons in a uniform positive neutralizing background, then we are modeling the homogeneous electron gas, or "jellium," a model for electrons in a solid. If m is the mass of the particles under study and Ze their charge, then $a_0 = \hbar^2/m(Ze)^2$ is a natural length scale, and $\mathrm{Ry} = \hbar^2/2ma_0^2$ the energy scale (the usual rydbergs, if the particles are electrons). The dimensionless ratio, $r_s = a/a_0$, where $a = (3V/4\pi N)^{1/3}$, is used to construct the dimensionless classical coupling parameter, $\Gamma = (Ze)^2/ak_BT = 2/r_sk_BT$. The classical OCP requires only Γ to express the equation of state. The quantum OCP requires an additional parameter, either r_s or k_BT. Also of interest is the ratio of the thermal de Broglie wavelength, λ_T, to a, $\lambda_T/a = (\hbar^2/mk_BT)^{1/2}/a = (\Gamma/r_s)^{1/2}$. Quantum exchange (particle statistics) is unimportant when $\lambda_T \ll a$.

Wigner [2] noted long ago that the electron gas would form a crystal at very low temperatures. In a very early computer simulation, Brush, Sahlin, and Teller [3] observed a transition in a 32 particle classical Monte Carlo simulation at $\Gamma_m = 125$. Hansen [4] and Pollock and Hansen [5] followed with an improved calculation, and found $\Gamma_m = 155 \pm 10$. Van Horn [6] used the empirical Lindemann ratio melting criterion to determine a transition at $\Gamma_m = 170 \pm 10$. Other studies have converged on the current estimate of $\Gamma_m = 172 - 178$ [7–10]. Application of pressure to the quantum solid results in melting [2,11].

Significantly less has been said regarding the quantum effects on the melting point of the OCP. Until very recently, classical studies were thought to be sufficient for most astrophysical systems, since the de Broglie wavelength, measured relative to the separation a, is less than unity. The OCP has so far been simulated at zero temperature by Ceperley and Alder [12] for both fermions and bosons [transition at $r_s^0 = r_s(T = 0) = 160$ for bosons and particles with Boltzmann statistics]. Hansen [4] and Pollock and Hansen [5] discussed quantum effects by including the first, order $\hbar^2$, term in the Wigner-Kirkwood expansion for the free energy. Higher order corrections were later added by Hansen and Viellefosse (HV) [13]. Iyetomi, Ogata, and Ichimaru [14] used the fluid corrections along with a quantum Monte Carlo simulation for the crystal phase to estimate the importance of quantum effects. Chabrier, Ashcroft, and DeWitt [15], however, have pointed out that, under typical white dwarf conditions, the expansion parameter proposed by Hansen and Viellefosse and later used by Iyetomi *et al.* is larger than one. Chabrier [16] has instead used a generalized Lindemann criterion [17] based on an analytic harmonic crystal model, interpolated between zero temperature and the classical regime, to find that, although the energies in both phases may be strongly affected by quantum effects, the transition is still close to the classical prediction over much of the region of interest. Nagata, Nagara, and Nakamura [18] used a new expansion scheme to add quantum corrections to the Slattery-Doolan-DeWitt (SDD) [7] fluid energies, along with path integral Monte Carlo (PIMC) calculations of the solid phase. Iida and Ichimaru [19] have also recently estimated the freezing transition for fermions at finite temperature using the Iyetomi *et al.* solid results and calculations of second-order exchange diagrams for the fluid phase.

We have used PIMC to study the state of the OCP at finite temperature, and thus directly calculated the importance of quantum effects in the two phases. The PIMC method allows us to simulate quantum systems at finite temperature with no uncontrolled approximations [20–23]. The long range nature of the Coulomb interaction presents a difficulty, but is tractable [5,24,25].

To locate the transition between the crystal and liquid phases in the OCP, we use two criteria: dynamical melt-

 0031-9007/96/76(24)/4572(4)$10.00

ing and free energy crossing. The dynamical melting criterion simply brackets the location of the phase transition between simulations in either phase by examining whether a given phase is stable. To determine the phase of each individual simulation, either observing the value of the total energy relative to its neighboring temperatures or examining the structure factor was enough. This method is simple, but many long simulations are needed to pinpoint the transition, metastability can be problematic, and the dependence on the size of the system is significant.

The free energy crossing (determined by thermodynamic integration of the total energies) can be more easily corrected for size dependence, as we discuss below. We have sampled many temperatures (in both phases) at four specific densities ($r_s = 1200, 200, 160, 100$), and various densities (again in both phases) at three fixed temperatures ($\beta = 18\,750, 23\,437.5, 37\,500$), as shown by the points in Fig. 1. The crossed points represent simulations in the crystal phase, and the open points the liquid phase.

In order to determine the dependence of the total energy upon the finite size of the system, we studied selected temperatures in the simulations at $r_s = 1200$ and 200. The crystal phase size dependence was observed to vary inversely with N and $r_s^{3/2}$. No temperature dependence was evident in the size correction term for the crystal phase, enabling us to extrapolate to the thermodynamic limit using the expression

$$E_N - E_\infty = -\frac{3.03(8)}{N r_s^{3/2}}. \quad (1)$$

For the liquid phase, we found instead that

$$E_N - E_\infty = [0.035(18) - 0.0018(1)\Gamma]/N r_s. \quad (2)$$

The crystal size dependence is within a standard deviation of that of Ceperley [25], and the liquid size dependence reduces to that of SDD [7] as $\Gamma \to 1$. The effect of the size dependence on the melting transition is taken into account by including the size correction term (appropriately integrated) in the free energy.

To determine the free energy we fit the total crystal energy with an anharmonic form,

$$(E - E_0)/N = a_0 + a_1/\Gamma^2 + a_2/\Gamma^3, \quad (3)$$

where $E_0/N = 1.79185/r_s$ is the energy of the ideal bcc lattice. A similar expression may be used to fit the liquid energy data at low temperatures. The exceptional case is for $r_s \leq 190$, where (for both the crystal and low temperature liquid) the fit was made by $(E - E_0)/N = a_0 + c/\Gamma^{3/2}$. This expression is more slowly varying in Γ than Eq. (3), and more accurately reflects the energy dependence at larger densities. Figure 2 shows our crystal energy data (points with error bars and solid lines) at several densities as a function of Γ. The solid points at zero temperature are the Monte Carlo values of Ceperley [25]. The dashed curves are the energies of the harmonic crystal model proposed by Chabrier [16]. The

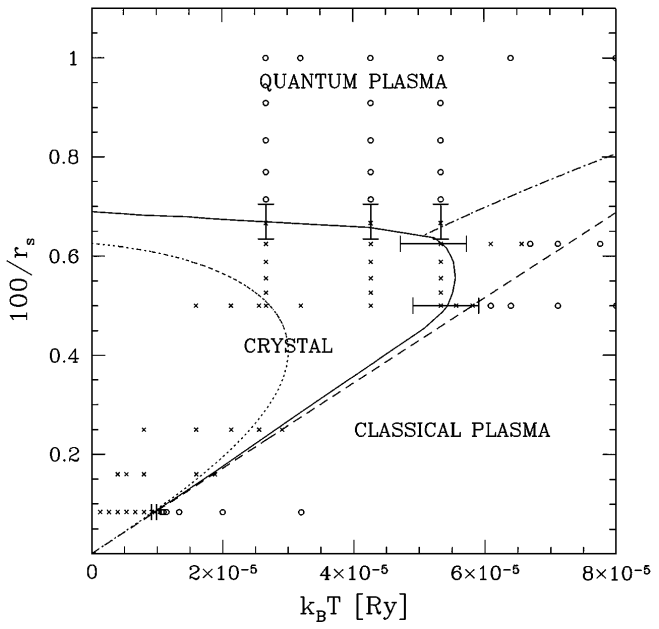

FIG. 1. The OCP phase diagram. The open circles are $N = 54$ simulations which remained in the liquid phase, while the crosses are simulations which remained in the crystal phase. The demarcation between these two sets of points marks the dynamical melting point. The dotted line is the predicted melting curve of Chabrier [16], and the dashed line is the classical melting point. The dash-dotted line is the projected superfluid–normal fluid transition temperature based upon that of ^{4}He [22]. Points with error bars are our PIMC melting points. The solid line is provided only to guide the eye.

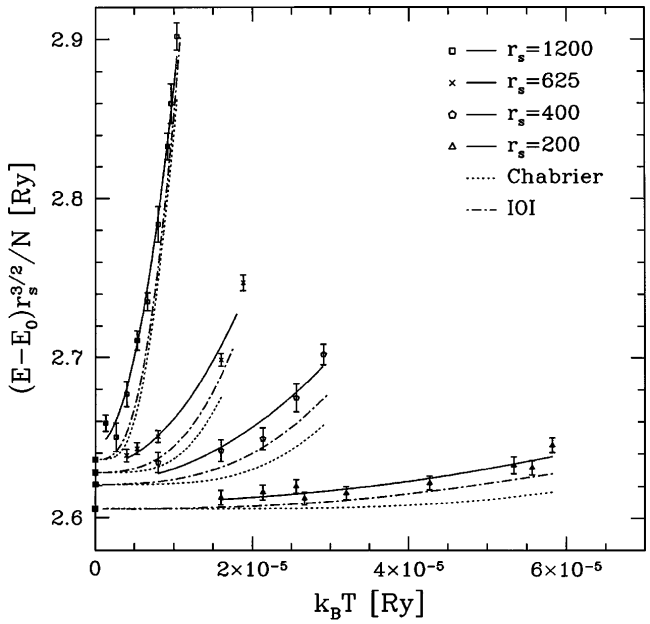

FIG. 2. A comparison of the PIMC crystal energies (points with error bars and solid lines) with the harmonic crystal model of Chabrier [16] (dotted lines) and the zero temperature Monte Carlo values of Ceperley [25] (filled squares). The calculations of Iyetomi *et al.* [14] (dot-dashed lines) lie between our results and those of the harmonic model. Note the scaling by $r_s^{3/2}$.

extrapolation of the present results to zero temperature is in good agreement with the previous zero temperature calculations (within error bars). We also note that the harmonic model is not adequate to describe the finite temperature energies, although it does appear to do well at extremely low temperature, and for densities where the total energy is very slowly varying with respect to temperature. The PIMC results of Iyetomi *et al.* [14] show a slight improvement over the harmonic model, and lie between the harmonic prediction and our results.

The liquid energies at constant density show a much stronger temperature dependence, so they become more challenging to fit. There is no satisfactory microscopic model of quantum liquids to use to obtain a simple expansion scheme, but we found that an expansion of the liquid energy in terms of $\Gamma^{1/4}$ works well for the range of densities and temperatures that we have explored,

$$(E - E_0)/N = \sum_{i=0}^{6} b_i \Gamma^{(i-4)/4}. \quad (4)$$

For low temperatures, a functional similar to Eq. (3) should instead be used for the liquid energy. Figure 3 plots our PIMC liquid energies as a function of Γ for several densities, in comparison with the classical results of SDD and the semiclassical calculations of HV. The departure from the classical fluid is clear, and occurs at higher temperatures (smaller Γ) as the density is increased (r_s is lowered). Note the instability of the semiclassical expression of Hansen and Vieillefosse [13] even at moderately large values of Γ, when the de Broglie wavelength becomes comparable to the average interparticle separation, well before the transition region is reached. Our PIMC liquid energies are in agreement with the classical Monte Carlo values of SDD at the highest temperatures. The corrections computed by Iida and Ichimaru [19] do not show the instabilities of the semiclassical corrections, but are more appropriate for fermions, and are not included in Fig. 3.

The freezing transition (determined using the free energies), before allowing for finite size effects, was consistent with the dynamical melting point observed in the simulations. We have found that size effects, which favor the crystal phase, shift the transition temperature by approximately 10% above the $N = 54$ melting point. This brings the transition to $\Gamma_m \simeq 175(7), 185(17), 240(23)$ for $r_s = 1200, 200, 160$, and $r_s \simeq 149(8)$ for all three constant temperature lines.

Figure 4 plots the Lindemann's ratio, γ, of the OCP crystal determined by the PIMC simulations, and compares it with Chabrier's harmonic model. Note the importance of anharmonic effects even at relatively low temperatures for the larger densities. The Lindemann ratio is more sensitive to these effects than is the total energy. Our results for the Lindemann ratio do not show finite size dependence within our statistical errors.

The slope of the melting curve can also be determined by using the Clausius-Clapeyron relation in conjunction with thermodynamic quantities found using PIMC. We work in the r_s^{-1}-T plane, since the uniform rigid background fixes the microscopic density, in contrast to the uncharged system, where pressure and temperature would be specified. The transition between liquid and solid is determined by the equivalence of the free energy, $F(r_s^{-1}, k_B T)$, in the two phases. The virial relation for

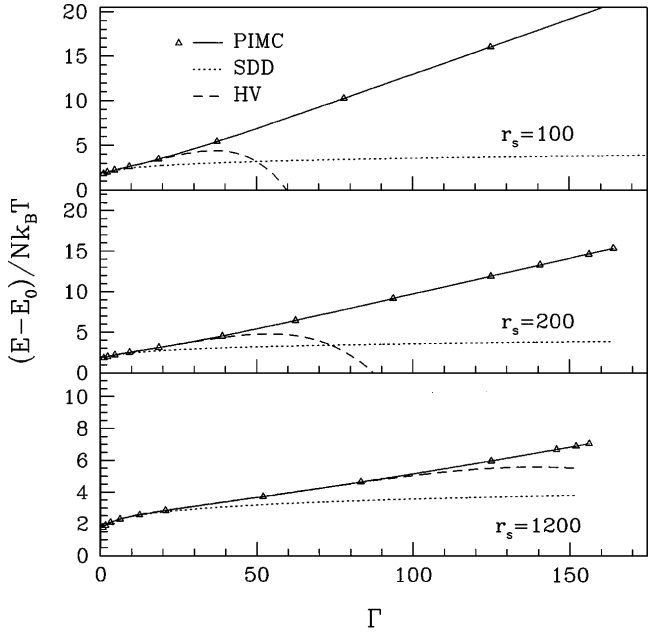

FIG. 3. The thermal excess energy in the OCP fluid phase (△ and solid lines), compared with the classical fluid simulations of SDD [7] (dotted lines), and the semiclassical calculations of HV [13] (dashed lines).

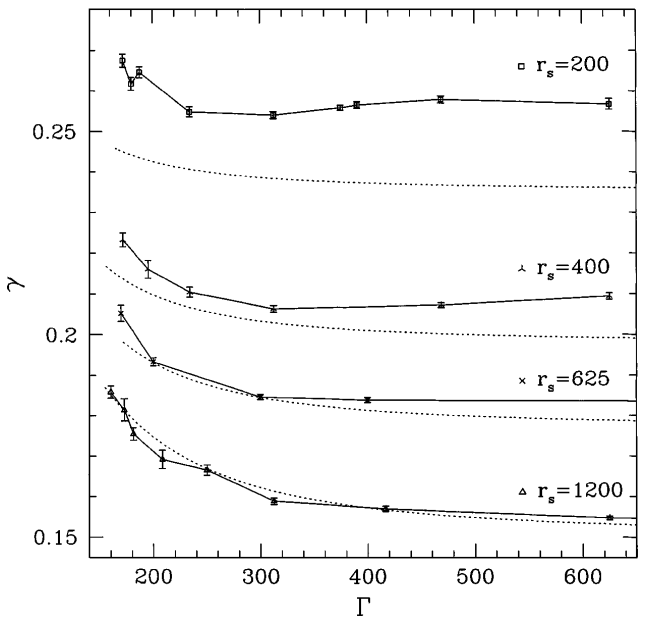

FIG. 4. The Lindemann ratio of the OCP crystal as a function of Γ for selected densities, compared with the harmonic crystal model of Chabrier [16] (dashed line). The classical value of the Lindemann ratio at melting is 0.155.

the OCP, $pV = (E + K)/3$, where p is the pressure and K the kinetic energy, implies that the transition line (with Bose, Fermi, or Boltzmann statistics) obeys the differential equation

$$\frac{d(2/r_s)}{d(k_BT)} = \Gamma \frac{\delta E_N}{\delta K_N + \delta E_N}, \tag{5}$$

where $\delta E_N = E_x/N - E_l/N$ and $\delta K_N = K_x/N - K_l/N$ are the changes in total and kinetic energy between the crystal (E_x, K_x) and liquid (E_l, K_l) phases. In the classical regime, $\delta K_N \ll \delta E_N$, so the slope of the melting curve (in these units) is $\Gamma = 175$. The first quantum correction to the slope is given by [13]

$$\frac{d(2/r_s)}{d(k_BT)} \simeq \Gamma\left[1 + \mathcal{O}\left(\frac{\Gamma^3}{r_s^2}\right) + \cdots\right]. \tag{6}$$

Eventually, a turning point is reached (in our PIMC data near $r_s = 160$), when $\delta E_N \simeq -\delta K_N$, and the slope becomes singular. Near the top of the phase diagram, $\delta E_N \to 0$, and the slope is very small. Table I lists our PIMC determined slope at $r_s = 1200$, 200, and 160 predicted by the above relation, as well as the energy differences δK_N and δE_N. We note that $\delta E_N \le 0$ over the complete phase diagram, while δK_N is positive and increasing as one follows the phase boundary from the classical to the quantum regime. This behavior indicates that the slope of the melting curve is negative (but very small) near the quantum $T = 0$ melting point.

The phase diagram illustrated in Fig. 1 summarizes our description of the liquid-crystal boundary in the OCP. Included in Fig. 1 are the size independent transition points from our OCP data, along with Chabrier's prediction. Our analysis finds the crystal phase more stable than that of Chabrier. From this phase diagram, we see a maximum melting temperature, $T^* = 6.0(5) \times 10^{-5}$ Ry, at a density of $r_s^* = 180(20)$. For the electron gas, this corresponds to $T^* = 9.5(8)$ K at $n^* = 2.8(9) \times 10^{17}\ e^-/\mathrm{cm}^3$, while for a carbon plasma, $T^* = 2.7(2) \times 10^8$ K at $\rho^* = 2.7(9) \times 10^{12}\ \mathrm{g/cm}^3$.

Quantum statistics, neglected here, will play a role in the region below the dash-dotted line in Fig. 1 indicating the onset of superfluidity for ^{4}He [given by $\lambda_T \ge \sqrt{1.6}\,\rho^{-1/3}$, or $r_s \le (3/4\pi)^{1/3}(3.2/k_BT)^{1/2}$], where particle statistics become important for a system of interacting bosons. For bosons there will be a triple point (crystal, normal fluid, and superfluid) located near the maximum melting temperature.

TABLE I. Parameters in the slope of the OCP melting curve, as determined by the Clausius-Clapeyron equation. At zero temperature [12], $\delta E_N = 0$, and $\delta K_N = 1.3(3) \times 10^{-4}$.

r_s	Γ_m	$\delta K_N \times 10^5$	$\delta E_N \times 10^5$	$d(2/r_s)/d(k_BT)$
1200	175	0.003(49)	−2.0(4)	175(4)
200	185	1.12(14)	−2.38(22)	423(38)
160	240	1.84(52)	−2.63(57)	800(800)

We have presented a PIMC study of the OCP freezing transition at finite temperature. We have found that the solid-liquid boundary is quite close to the classical line for an extended portion of the phase diagram, far further than expected based upon a consideration of the generalized Lindemann melting criterion. The Lindemann criterion fails due to the large anharmonic effects present in the crystal phase. Although the quantum effects are relatively large near the transition, quantum contributions to the two phases are nearly equal, making the classical prediction of the melting point valid for a large portion of the OCP phase diagram.

This work was supported by ONR Grant No. N00014-93-1029, the National Center for Supercomputing Applications (NCSA), and the Department of Physics at the University of Illinois at Urbana-Champaign. Computations were performed at NCSA and the Cornell Theory Center. We thank H. E. DeWitt for suggesting this calculation.

[1] E. E. Salpeter, Astrophys. J. **3**, 669 (1961).
[2] E. Wigner, Phys. Rev. **46**, 1002 (1934).
[3] S. G. Brush, H. L. Sahlin, and E. Teller, J. Chem. Phys. **45**, 2102 (1966).
[4] J. P. Hansen, Phys. Rev. A **8**, 3096 (1973).
[5] E. L. Pollock and J. P. Hansen, Phys. Rev. A **8**, 3110 (1973).
[6] H. M. Van Horn, Phys. Lett. **28A**, 706 (1969).
[7] W. L. Slattery, G. D. Doolan, and H. E. DeWitt, Phys. Rev. A **21**, 2087 (1980); **26**, 2255 (1982).
[8] D. Dubin, Phys. Rev. A **42**, 4972 (1990).
[9] G. S. Stringfellow, H. E. DeWitt, and W. L. Slattery, Phys. Rev. A **41**, 1105 (1990).
[10] R. T. Farouki and S. Hamaguchi, Phys. Rev. E **47**, 4330 (1993).
[11] D. A. Kirzhnits, Sov. Phys. JETP **11**, 365 (1960).
[12] D. M. Ceperley and B. J. Alder, Phys. Rev. Lett. **45**, 566 (1980).
[13] J. P. Hansen and P. Viellefosse, Phys. Lett. **53A**, 187 (1975).
[14] H. Iyetomi, S. Ogata, and S. Ichimaru, Phys. Rev. B **13**, 11 703 (1993).
[15] G. Chabrier, N. W. Ashcroft, and H. E. DeWitt, Nature (London) **360**, 48 (1992).
[16] G. Chabrier, Astrophys. J. **414**, 695 (1993).
[17] R. Mochkovitch and J. P. Hansen, Phys. Lett. **73A**, 35 (1979).
[18] H. Nagata, Y. Nagara, and T. Nakamura, Phys. Rev. A **36**, 1859 (1987).
[19] K. Iida and S. Ichimaru, Phys. Rev. B **52**, 7278 (1995).
[20] R. P. Feynman, Phys. Rev. **91**, 1291 (1953).
[21] E. L. Pollock and D. M. Ceperley, Phys. Rev. B **30**, 2555 (1984).
[22] D. M. Ceperley, Rev. Mod. Phys. **67**, 279 (1995).
[23] N. Metropolis, A. Rosenbluth, M. N. Rosenbluth, A. Teller, and E. Teller, J. Chem. Phys. **21**, 1087 (1953).
[24] V. Natoli and D. M. Ceperley, J. Comp. Phys. **117**, 171 (1995).
[25] D. M. Ceperley, Phys. Rev. B **18**, 3126 (1978).